Periodica Polytechnica Chemical Engineering, 69(2), pp. 260–272, 2025

Preparation and Adsorption Efficiency of Mango Waste-derived Biosorbents for Lead Removal in Water

Karl Philip G. Roderno[1], Ariadna L. Agoto[1], Quennae Mae D. Cariño[1], Pretzel Jade R. Padilla[1], Rugi Vicente Rubi[1,2*]

[1] Department of Chemical Engineering, College of Engineering, Adamson University, 900 San Marcelino St., Ermita, 1000 Manila, Philippines
[2] Adamson University Laboratory for Biomass, Energy and Nanotechnology (ALBEN), Adamson University, 900 San Marcelino St., Ermita, 1000 Manila, Philippines
[*] Corresponding author, e-mail: rugi.vicente.rubi@adamson.edu.ph

Received: 10 December 2024, Accepted: 28 March 2025, Published online: 15 May 2025

Abstract

The need to mitigate heavy metals contamination in the water environment using sustainable adsorbents has gain much attention recently due to compliance to sustainable development goals (SDGs) in the global context. This study explored the potential of Philippine mango (*Mangifera indica* L.) waste – specifically the peel, seed, and pit – as bioadsorbents for Pb^{2+} removal from synthetic wastewater. The bioadsorbents were prepared through drying and grinding, followed by chemical modification with HNO_3 and NaOH. Characterization using Fourier-transform infrared (FTIR) spectroscopy and scanning electron microscopy (SEM) revealed surface functional groups and structural changes. Adsorption capacity was quantified using atomic absorption spectroscopy (AAS), and batch experiments were conducted with UV-Vis spectrophotometry. The untreated mango seed (UMSD) exhibited the highest Pb^{2+} adsorption capacity, exceeding 42.10 mg/g. Adsorption efficacy increased with higher initial Pb^{2+} concentrations, with untreated seed outperforming modified variants. Kinetic studies indicated rapid lead uptake, reaching equilibrium within 30 min. The adsorption data were best described by the Langmuir isotherm model, suggesting monolayer adsorption, while pseudo-second-order kinetics indicated that chemical bonding was the dominant mechanism. These results underscore the potential of UMSD as a cost-effective and sustainable bioadsorbent for lead removal in wastewater treatment, particularly in the Philippines.

Keywords

mango waste, bioadsorbent, Pb^{2+} removal, adsorption capacity, wastewater treatment

1 Introduction

Sustainable resource management attains a global emphasis as an effective treatment and management of wastewater that facilitates on the mitigation of environmental degradation and safeguarding public health that play significant role in achieving ecological and human sustainability. The rise of industrialization and globalization has led to an increasing demand for clean water, while simultaneously contributing to the discharge of large volumes of effluent wastewater. Many industrial effluents contain hazardous pollutants, including dyes, heavy metals, and aromatic compounds, which pose significant threats to water quality and ecosystem health. Due to their small size, stability, and non-biodegradability, removing these molecular pollutants from wastewater remains a significant challenge [1].

Industries such as battery manufacturing, mining, metal plating, electroplating, textiles, and petroleum refining are major sources of lead pollution. Lead concentrations in industrial wastewater can vary significantly depending on the industry and process involved. Lead-acid battery production, in particular, generates substantial lead-contaminated wastewater, often combined with sulfuric acid (H_2SO_4), which lowers pH and increases acidity. Improper disposal of lead-acid batteries results in the leaching of lead and sulfuric acid into the environment, with potential infiltration into groundwater systems, severely compromising drinking water quality and posing serious health risks [2].

Various conventional methods have been employed to remove lead and other heavy metals from wastewater,

Cite this article as: Roderno, K. P. G., Agoto, A. L., Cariño, Q. M. D., Padilla, P. J. R., Rubi, R. V. "Preparation and Adsorption Efficiency of Mango Waste-derived Biosorbents for Lead Removal in Water", Periodica Polytechnica Chemical Engineering, 69(2), pp. 260–272, 2025. https://doi.org/10.3311/PPch.39523

including precipitation, flocculation, activated sludge treatment, photodegradation, and phytoremediation. However, these techniques often exhibit limitations such as incomplete removal of pollutants, high operational costs, and secondary waste generation. Adsorption using bioadsorbents has emerged as an efficient and cost-effective alternative due to its availability, environmental friendliness, and high adsorption capacity [3].

Several studies have explored bioadsorbents derived from agricultural waste for heavy metal removal. For instance, banana peel exhibited an adsorption capacity of 22.42 mg/g for Pb^{2+} ions [4], while mango seed (MSD) powder showed effective heavy metal adsorption due to its rich lignocellulosic composition [5]. Other fruit wastes such as orange peels, coconut husks, and sugarcane bagasse have demonstrated promising results for lead adsorption, with capacities ranging from 10 mg/g to 50 mg/g, depending on pre-treatment methods applied [6]. Biosorbents from raw apple waste and extracted apple waste significantly have a maximum adsorption capacity of 44.6 and 48.6 mg/g respectively [7]. Pre-treatments such as chemical activation (acid/base treatment), thermal modification, and carbonization have been utilized to enhance the retention capacity of these bioadsorbents by increasing surface area and functional group availability [8].

Mangifera indica L. (Philippine mango) is one of the most widely cultivated fruits worldwide, yet only about 20% of mangoes are processed into products, leaving 35% to 60% of the fresh fruit as waste [5, 9]. Mango fruit wastes, including peels, seeds, and pits, contain high amounts of pectin, cellulose, and carboxyl functional groups, which have strong binding properties for metal cations. Studies have reported that mango peel (MPL) can remove Cu^{2+}, Ni^{2+} and Zn^{2+} ions with an adsorption capacity of approximately 46.09, 39.75, and 28.21 mg/g, respectively [10].

Regulatory frameworks emphasize the need for industries to minimize toxic discharges to protect public health and ecosystems. The Philippines enforces stringent water quality standards through Department of Environment and Natural Resources (DENR) administrative order (DAO) No. 2021-19, which sets specific effluent limits for lead and other pollutants to prevent water contamination [11, 12]. Given the urgent need for sustainable and cost-effective wastewater treatment technologies, utilizing mango fruit waste as a bioadsorbent presents a promising solution for lead removal.

This study aims to assess the potential of mango-derived bioadsorbents, specifically peels, seeds, and pits, for Pb^{2+} ion adsorption. The novelty of this research lies in the comparative evaluation of different mango waste components, their adsorption capacities, and the effect of various pre-treatment methods on their efficiency. By providing an eco-friendly and low-cost approach to lead removal, this study contributes to sustainable waste valorization and enhanced wastewater treatment technologies.

2 Methodology

2.1 Chemicals

The $Pb(NO_3)_2$ and ethylenediaminetetraacetic acid (EDTA) were procured from DKL Laboratories, while the NaOH, HNO_3, and deionized water were purchased from the Adamson University Chemistry Laboratory. Ripe carabao mango wastes sourced in Indang, Cavite were utilized to ensure consistency.

2.2 Preparation of adsorbents

The peels, seeds, and pits were thoroughly washed with tap water to remove dust and impurities. It is then dried in an oven to ensure complete moisture removal. Once dried, they were ground into a fine powder using a blender and sieved through a 100-mesh screen to achieve a consistent particle size as shown in Fig. 1. For the modification phase, acid and base solutions were utilized to enhance the active surface properties of the bioadsorbents. Specifically, 1 M HNO_3 and 1 M NaOH solutions were prepared for this purpose. A quantity of 15 g of MPL, MSD, and mango pit (MPT) samples were placed in 500 mL Erlenmeyer flasks, each containing 250 mL of the modified solution (acid and bases). The samples were shaken using rotary shaker bath for 1 h until fully immersed and left to react for three days. Afterward, the mixtures were filtered using Whatman No. 1 (pore size 11 μm) to separate the modified bioadsorbents, which were then dried under ambient conditions.

2.3 Characterization of bioadsorbent

The functional groups present on the MPLs, MSDs, and MPTs were analyzed using Fourier-transform in-

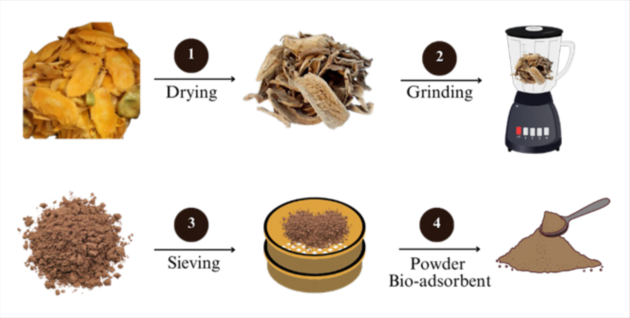

Fig. 1 Process of treatment of the MPL, MSD, and MPT

frared (FTIR) spectroscopy, with measurements taken across the range of 4000 to 400 1/cm. This technique enabled detailed identification of the specific functional groups on the surface of these materials [13]. The dried powder sample of untreated mango peel (UMPL), untreated mango seed (UMSD), and untreated mango pit (UMPT), acid-treated mango peel (AMPL), acid-treated mango seed (AMSD), acid-treated mango pit (AMPT), base-treated mango peel (BMPL), base-treated mango seed (BMSD), and base-treated mango pit (BMPT) were directly place on the diamond reflection attenuated total reflectance (ATR) device of the FTIR. Additionally, the surface morphology of the mango fruit wastes was examined with scanning electron microscopy (SEM) (Phenom XL, Thermo Scientific) under these conditions: the acceleration voltage (10 kV) and the magnification between 20,000 to 50,000, provide high-resolution images to visualize and assess the structural characteristics and texture of the MPL, MSD, and MPT absorbents (untreated and treated with acid and base).

2.4 Preparation of lead solutions for atomic absorption spectroscopy (AAS)

The stock solution of Pb^{2+} ions in this study was prepared by dissolving 160 mg of $Pb(NO_3)_2$ in 1 L of deionized water, by sequential dilution calibration concentrations of 20, 40, 60, 80, 100, 120, 140, and 160 ppm were prepared. To ensure experimental consistency, all adsorbates utilized in the study were sourced from this singular stock solution of 160 ppm and then diluted to form the other concentrations needed. This approach guarantees uniformity in the Pb^{2+} ion concentration across all experimental conditions, thereby enhancing the reliability and comparability of the results.

2.5 AAS adsorption study

For sample preparation, 0.04 g of each bioadsorbent was added to a centrifuge tube with 20 mL of 100 ppm lead solution. These mixtures were agitated in an orbital shaker at 400 rpm for 120 min and then filtered using a suction apparatus [14]. The filtrate is filtered using Whatman No. 1 (pore size 11 μm) and sequential filtration with cellulose membrane syringe filter (pore size 0.45 μm). The resulting filtrate underwent a digestion process with 5.0 mL of concentrated nitric acid (HNO_3), and heated on a hot plate at 50 °C for less than 1 h.

After cooling to room temperature, the digested samples were deionized water to a final volume of 50 mL.

The initial and final concentrations of lead in the solutions, measured before and after the experiment, were analyzed AAS (AA-7000, Shimadzu, Italy). The lead removal efficiency of the bioadsorbent was calculated using Eq. (1):

$$\text{Lead removal efficiency}\left(\%\right)=\frac{C_i-C_f}{C_i}\times 100, \tag{1}$$

where C_i represents the initial concentration of the lead solution, and C_f denotes the concentration of lead remaining in the solution after the adsorption process.

2.6 UV-Vis spectra

The experiment utilized a wavelength range of 210 to 300 nm to analyze the lead-EDTA complex, a choice made to thoroughly capture its absorption characteristics. This range is ideal for detecting the complex's absorbance, as lead-EDTA typically shows significant absorption within this interval (UV-1900i Plus, double-beam UV-Vis spectrophotometer). The lower end of the spectrum, starting at 210 nm, allows for the observation of initial absorption features, while extending up to 300 nm ensures the inclusion of more pronounced absorption peaks. This comprehensive approach facilitates a detailed analysis of the complex's electronic transitions and interactions with light.

2.7 Batch adsorption experiment

The experimental procedure involved systematically varying key parameters (contact time and concentration of lead) with the initial adsorbent loading of 0.3 g, initial pH of 6–7, and an orbital shaker speed of 160 rpm across all tests [15, 16]. A series of assessment of the relationship of the contact time and the concentration of the lead are tested. Initially, with the contact time held constant at 75 min, Pb^{2+} ion concentrations were varied at 25, 50, 75, 100, 125, and 150 ppm. This assessed the influence of different Pb^{2+} ion concentrations on the adsorption capacity of the mango-based bioadsorbent over time. Subsequently, the Pb^{2+} ion concentration was kept constant at 150 ppm while the contact time was adjusted to 5, 15, 30, 45, 60, and 75 min. This allowed for the evaluation of how different interaction durations impacted the adsorption efficiency of the mango-derived bioadsorbent.

After each designated contact period, the solutions were filtered to remove the bioadsorbent from the treated liquid. The pH of the filtrate was then adjusted with either 1 M NaOH or 1 M HCl, as required. Subsequently, 1.5 mL of 0.5 M EDTA was added. Adjusting the pH in this way enhanced the chelating effectiveness of EDTA, allowing for precise detection and measurement of any remaining Pb^{2+} ions.

2.8 Isotherm models

The isotherm experiment was determined with these following experimental parameters: bioadsorbent loading of 0.3 g/L, the initial concentration of Pb^{2+} ion 25, 50, 75, 100, 125, and 150 ppm, under pH 6–7, with contact time of 5, 15, 30, 45, 60, and 75 min at 25 °C ± 5. The data were employed to fit the Langmuir and Freundlich isotherm models to characterize the biosorption process. The Langmuir isotherm model assumes that adsorption takes place in a monolayer on a surface with uniform adsorption energy across all sites. This model presumes that each site can hold only one adsorbate molecule and that there are no interactions between adsorbate molecules [17]. The linear form of the Langmuir equation for adsorption can be expressed as:

$$\frac{C_e}{q_e} = \frac{1}{K_L q_{\max}} + \frac{C_e}{q_{\max}}, \tag{2}$$

where q_e represents the amount of adsorbate adsorbed by a unit mass of the adsorbent, K_L is the Langmuir constant related to the adsorption coefficient, $q_{\max}$ denotes the monolayer adsorption capacity, and C_e is the final concentration of the metal in the solution.

The Freundlich isotherm model describes adsorption on a heterogeneous surface with varying affinities for the adsorbate. Unlike the Langmuir model, it assumes that adsorption sites have different energies and that adsorption occurs on a surface with a non-uniform distribution of binding sites. The linear form of the Freundlich equation can be expressed as:

$$\ln q_e = \ln K_F + \frac{1}{n} \ln C_e, \tag{3}$$

where K_F is the Freundlich constant indicating the adsorption capacity, and n is a dimensionless constant that describes the adsorption intensity.

2.9 Kinetic models

In the kinetic model experiments, the following parameters were used to augment the suitable model for the mange adsorbents: bioadsorbent loading of 0.3 g/L, the initial concentration of Pb^{2+} ion 25, 50, 75, 100, 125, and 150 ppm, under pH 6–7, with contact time of 5, 15, 30, 45, 60, and 75 min at 25 °C ± 5. The pseudo-first-order kinetic model simplifies the kinetics of a reaction by assuming a constant concentration of a second reactant or catalyst, making it appear as a first-order reaction. This simplification aids in analysis and determination of an apparent rate constant:

$$\ln\left(q_e - q_t\right) = \ln q_e - K_1 t, \tag{4}$$

where q_e and q_t are the adsorption capacity at equilibrium and a specific time, respectively. The rate at which adsorption occurs is characterized by the rate constant K_1.

The pseudo-second-order kinetic model assumes that the rate of adsorption is proportional to the square of the difference between the equilibrium adsorption capacity and the amount adsorbed at a given time and can be expressed as:

$$\frac{t}{q_e} = \frac{1}{K_2 q_e^2} + \frac{1}{q_e}, \tag{5}$$

where q_e and q_t are the adsorption capacity at equilibrium and a specific time, respectively. The rate constant K_2 for the pseudo-second-order adsorption process.

3 Results and discussion

3.1 Preparation of the mango bioadsorbents

The MPL, MSD, and MPT underwent a two-week sun-drying process after being thoroughly washed. Subsequently, it was finely cut into small fragments and processed using a blender. The resulting mixture of MPL, MSD, and MPT was sieved through a 100-mesh screen (Fig. 2). To chemically modify the bioadsorbents, 1 M HNO_3 was utilized for acid treatment (Fig. 3), while 1 M NaOH was employed for base treatment. Base-treatment MPL, MSD, and MPT are represented in Fig. 4. Notably, among the produced MPL bioadsorbents, the BMPL bioadsorbent exhibited the darkest coloration. Additionally, both AMSD (Fig. 3) and BMSD (Fig. 4) bioadsorbents displayed a significant change in color compared to the UMSD (Fig. 2) bioadsorbent. Conversely, the BMPT bioadsorbent exhibited a yellowish hue, contrasting with the reddish color of the AMPT bioadsorbent and the pale appearance of the UMPT bioadsorbent. An investigation conducted by Tsaniatri and Hargono [9] established that nitric acid modification enhances the hydroxyl group content in cellulose, leading to an increase in both adsorption capacity and efficiency for Pb^{2+} adsorption. Similarly, in the study of Huang et al. [18] demonstrated that sodium hydroxide modification results in an augmented presence of amino and hydroxyl groups, facilitating Pb^{2+} adsorption through an expansion of surface area and the creation of a porous structure.

3.2 FTIR spectroscopy analysis

To determine the functional groups in the different biosorbents (Figs. 5 and 6) before and after adsorption of Pb^{2+} in water, Fourier Transform Infrared Spectroscopy (Spectrum Two FT-IR Spectrometer, $LiTaO_3$ detector) was employed. The FTIR spectra of MPL (UMPL, BMPL, AMPL) and MSD waste (UMSD, BMSD, AMSD) reveal distinct

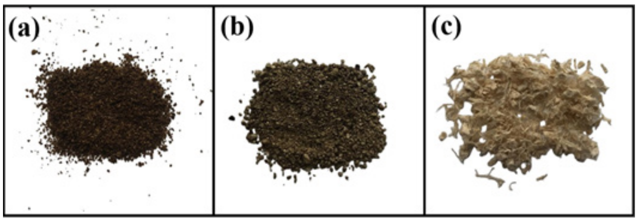

Fig. 2 Untreated untreated mango bioadsorbent: (a) UMPL; (b) UMSD; (c) UMPT

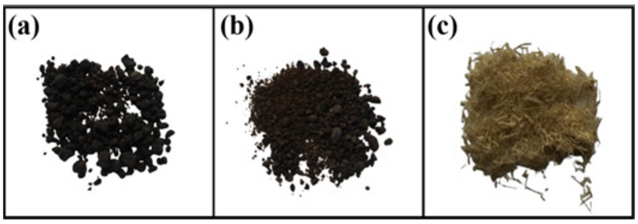

Fig. 3 Acid-treated mango bioadsorbent: (a) AMPL; (b) AMSD; (c) AMPT

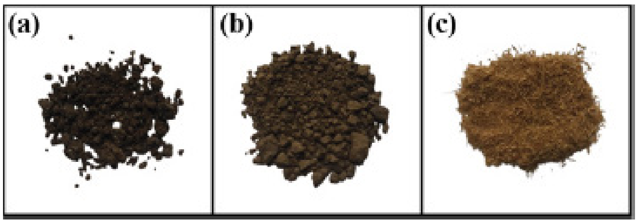

Fig. 4 Base-treated mango bioadsorbent: (a) BMPL; (b) BMSD; (c) BMPT

alterations in the functional groups before and after adsorption, particularly in the O–H, C–H, and C=O stretching regions. Prior to adsorption, the O–H stretching was evident in MPL waste, with characteristic peaks around 3332 1/cm for UMPL, 3338 1/cm for BMPL, and 3331 1/cm for AMPL. Similarly, MSD waste exhibits O–H stretching peaks at 3332 1/cm for UMSD, 3281 1/cm for BMSD, and 3330 1/cm for AMSD [5, 13].

Upon adsorption, represented in Fig. 6, there is a pronounced broadening of the O–H stretching band within the 3000–3500 1/cm range for both types of waste. In MPL waste, new peaks emerge at 1714 1/cm for UMPL and 1715 1/cm for AMPL, while BMPL shows negligible changes in the C=O stretching intensity, indicating minimal interaction involving carbonyl groups. Conversely, in MSD waste, new peak intensities are observed at 1729 1/cm for UMSD, 1745 1/cm for BMSD, and 1737 1/cm for AMSD, suggesting the formation of new functional groups or enhanced interactions post-adsorption. The C–H stretching bands remain relatively unchanged, with peaks consistently observed at the range of 2920 1/cm for UMPL and UMSD, 2922 1/cm for AMPL, and 2922 1/cm for BMSD, indicating stable C–H bond environments. Notably, MPT waste (UMPT, BMPT, AMPT) exhibits only slight broadening in the O–H stretching region after adsorption, with no significant C=O stretching observed, further suggesting limited involvement of carbonyl groups in the adsorption process.

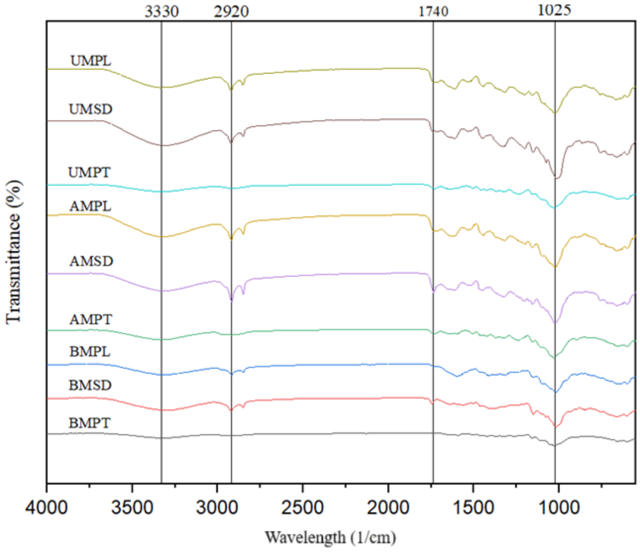

Fig. 5 FTIR spectra before adsorption

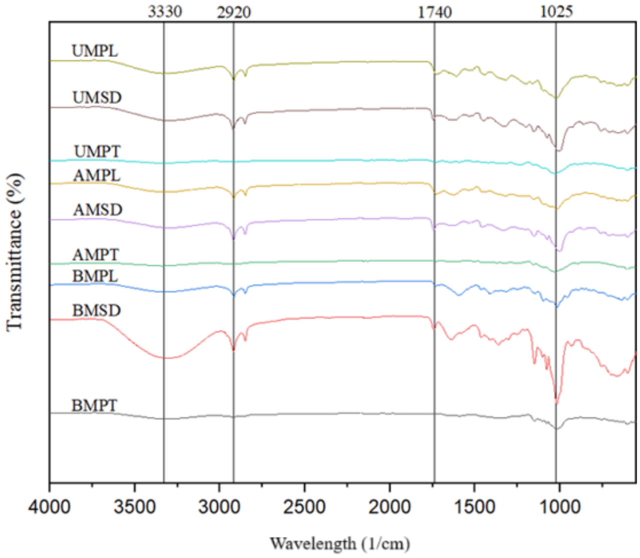

Fig. 6 FTIR spectra after adsorption

The FTIR spectra of the nine bioadsorbents, both before and after the adsorption of Pb^{2+}, highlight the functional groups present in the bioadsorbents. The slight stretch observed in the FTIR spectrum of mango bioadsorbents before adsorption indicates the presence of hydroxyl (O–H) groups around 3000–3500 1/cm [5]. Post-adsorption, the O–H peak broadens within the 3000–3500 1/cm range, and new peak intensities are observed, indicating the presence of carbonyl (C=O) groups. However, the absence of peak changes in some cases suggests the lack of C=O groups [19].

Additionally, the intensity of the C=O group increases after adsorption. The carboxyl group, known for its predominant role in metal ion adsorption [20], likely contributes to the observed changes. The shifts in transmittance and wavelength of the mango bioadsorbents in the FTIR spectra following lead adsorption suggest the involvement of hydroxyl and carboxyl groups in the adsorption process.

3.3 SEM analysis

The SEM micrographs of MPL, MSD, and MPT bioadsorbents provide an in-depth look at their surface structures before and after the adsorption of a 100 ppm $Pb(NO_3)_2$ solution (Figs. 7 and 8, respectively). Initially, UMPLs were characterized by a distinctly rough texture, marked by visible cracks and a fibrous structure. This roughness

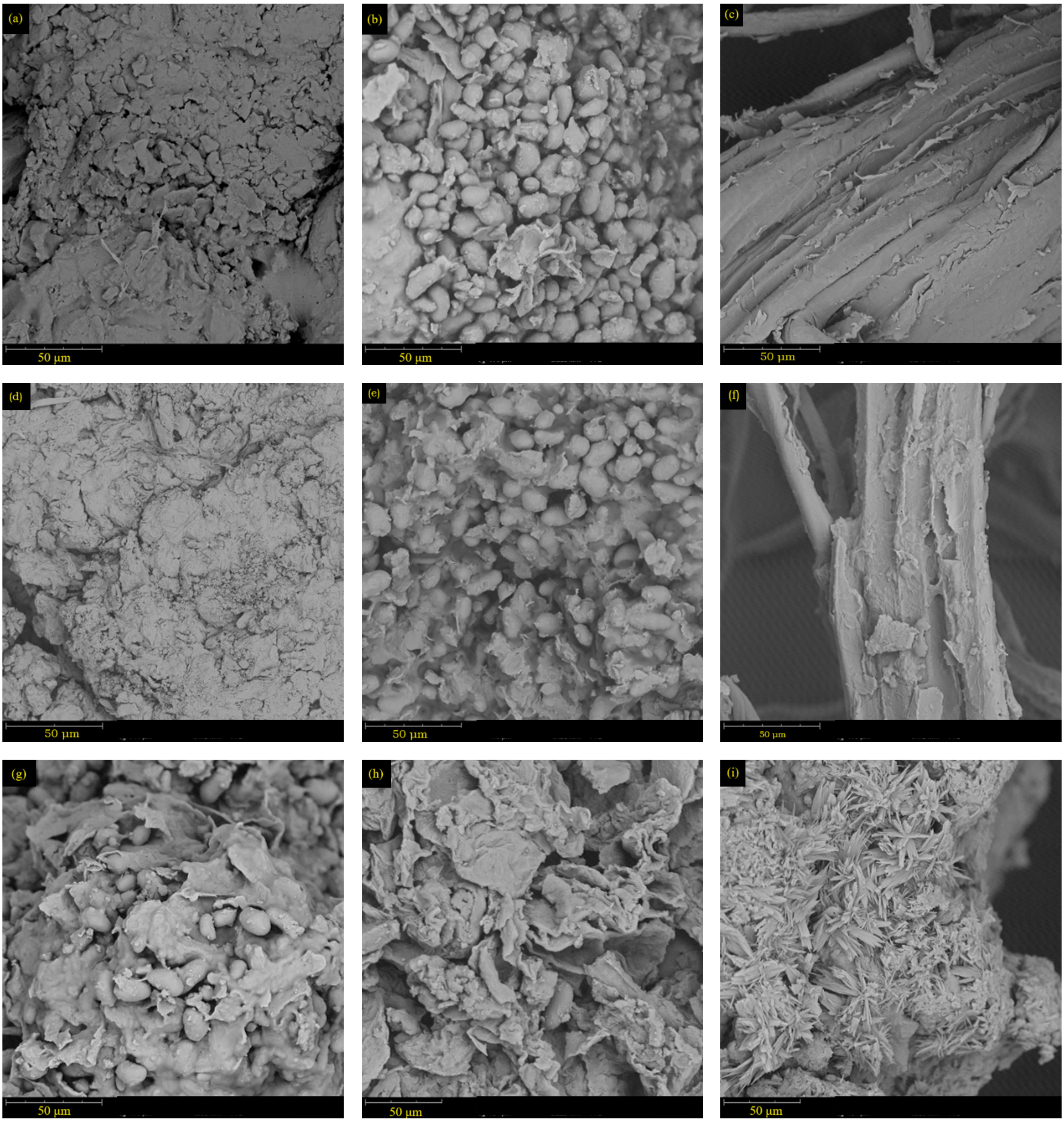

Fig. 7 SEM results of the synthesized mango bioadsorbents before adsorption: (a) UMPL; (b) UMSD; (c) UMPT; (d) AMPL; (e) AMSD; (f) AMPT; (g) BMPL; (h) BMSD; (i) BMPT

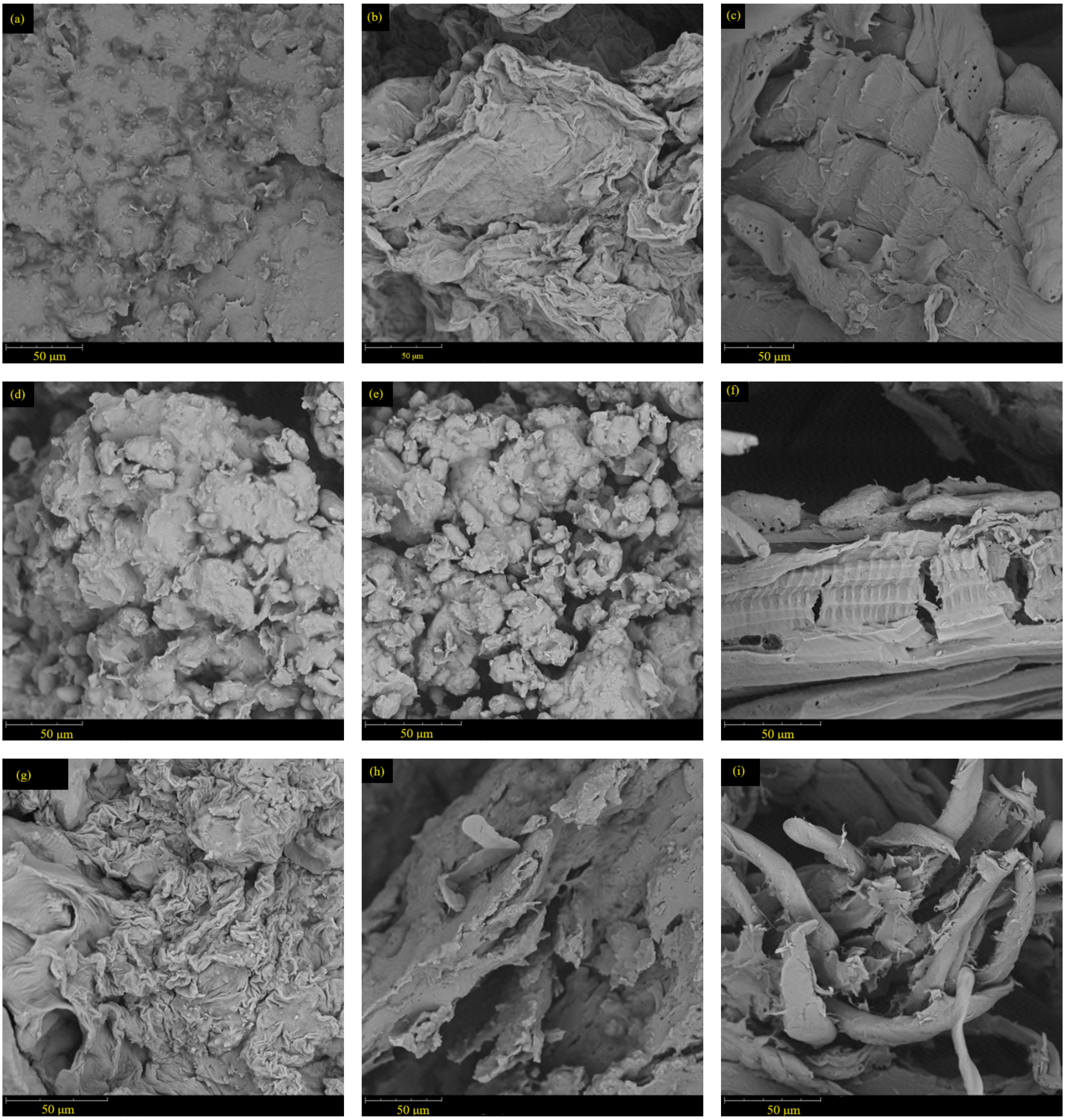

Fig. 8 SEM results of the synthesized mango bioadsorbents after adsorption: (a) UMPL; (b) UMSD; (c) UMPT; (d) AMPL; (e) AMSD; (f) AMPT; (g) BMPL; (h) BMSD; (i) BMPT

was consistent with prior study that documented the uneven surface texture of UMPLs [21]. These irregularities are believed to be significant in their role as adsorbents because the rough, fibrous texture may provide more surface area and potential sites for adsorption. In contrast, UMSDs displayed a more compact, fibrous structure with fewer visible pores compared to the peels.

Although the seeds were somewhat smoother, they still showed surface irregularities. This indicates a different surface texture that may influence their adsorptive properties. MPTs, on the other hand, exhibited a flake-like structure with numerous spots and holes. This particular morphology suggests that the pits have a higher surface area for potential adsorption and may be more effective at trapping Pb^{2+} ions within these cavities, as highlighted in earlier research [22].

Initially, UMPLs were characterized by a distinctly rough texture, marked by visible cracks and a fibrous structure. This roughness was consistent with prior studies that documented the uneven surface texture of UMPLs [21]. These irregularities are believed to be significant in their role as adsorbents because the rough, fibrous texture may provide more surface area and potential sites for adsorption. In contrast, UMSDs displayed a more compact, fibrous structure with fewer visible pores compared to the peels. Although the seeds were somewhat smoother, they still showed surface irregularities.

This indicates a different surface texture that may influence their adsorptive properties. MPTs, on the other hand, exhibited a flake-like structure with numerous spots and holes. This particular morphology suggests that the pits have a higher surface area for potential adsorption and may be more effective at trapping Pb^{2+} ions within these cavities, as highlighted in earlier research [10].

After the adsorption of Pb^{2+}, notable changes in the surface morphology of the bioadsorbents were observed. The UMPL, UMSD, and UMPT bioadsorbents retained their initial roughness and irregularities, indicating minimal impact of Pb^{2+} adsorption on their surface texture. In contrast, bioadsorbents pre-treated with 1 M HNO_3 and 1 M NaOH exhibited a pronounced reduction in surface roughness following Pb^{2+} adsorption. This significant alteration in surface texture suggests a decrease in the available surface area for adsorption, potentially implying diminished adsorptive properties of the chemically treated bioadsorbents. These changes may result from structural modifications or partial pore collapse induced by the chemical treatments. Furthermore, the observed reduction in adsorptive properties highlights the potential trade-offs between chemical activation and adsorption efficiency.

3.4 Effect of chemical treatment on Pb^{2+} adsorption efficacy

The AAS results, shown in Fig. 9, provided the equilibrium concentration data for all nine bioadsorbent samples. These results confirm the findings from FTIR and SEM analyses, which indicated the presence of functional groups and surface modifications that contributed to the bioadsorbents' performance.

MSD bioadsorbents showed the highest efficacies, with UMSD demonstrating the highest lead adsorption capacity at 42 mg/g, followed by BMSD at 38 mg/g, and UMPL at 37 mg/g. These results were corroborated by the FTIR spectroscopy data, which provided insights into the functional groups present on the bioadsorbent surfaces. In contrast, amples showed less pronounced changes in their FTIR spectra after adsorption, aligning with their lower removal efficiencies observed in the AAS analysis. The SEM analysis further supported these findings by revealing the surface morphology of the bioadsorbents. MSDs exhibited a complex porous structure with a large surface area, likely contributing to their superior adsorption performance. The peel samples showed a fibrous structure with some surface irregularities, while the pit samples displayed a flake-like structure with visible pores. Based on this comprehensive analysis, MSDs emerged as the optimal choice for bioadsorbents, with UMSD and BMSD demonstrating the highest adsorption capacities.

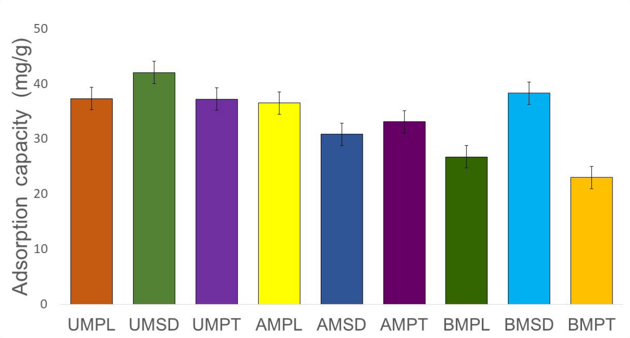

Fig. 9 Adsorption capacity of all samples (the equilibrium conditions is 100 ppm lead concentration, 0.04 g bioadsorbent dosage, 400 rpm mixing rate, 120 min contact time, and pH range of 5–6.5)

The superior performance of UMSD compared to BMSD suggests that the natural state of MSD waste possesses excellent adsorptive properties for lead ions. However, the base treatment still showed potential for enhancing adsorption capacity, as evidenced by the higher efficacy of BMSD compared to other treated samples. The AMSD showed a somewhat lower but still significant removal efficacy of 31 mg/g. This performance difference, observed under identical optimal conditions for all bioadsorbents, suggests that the acid treatment altered the bioadsorbent's surface properties or structure in ways that moderately affected its adsorption capacity. The acid treatment likely modified the surface functional groups of the MSD biomass, potentially resulting in altered surface charge distribution, changes in the pore structure or specific surface area, and modification of functional groups such as carboxyl, hydroxyl, or amino groups, which play crucial roles in metal ion binding. This suggests that even with surface modifications, the inherent properties of MSD biomass that make it effective for lead adsorption are largely retained. The observed differences in performance among UMSD, BMSD, and UMPL under optimal conditions provide valuable insights into how various treatments can affect the adsorption properties of MSD-based adsorbents. In conclusion, based on the AAS results corroborated by FTIR and SEM analyses, UMSD and BMSD were selected as the optimal bioadsorbents for further investigation in batch adsorption studies. This selection promises to yield valuable insights into the potential of MSD waste as an efficient, cost-effective, and environmentally friendly solution for lead removal from aqueous solutions.

3.5 Influence of varying initial lead concentrations

Fig. 10 also highlights that UMSD consistently outperforms BMSD in terms of adsorption capacity, a finding corroborated by the AAS results. Specifically, at a lead concentration of 150 ppm, the adsorption capacity of UMSD is 46 mg/g, compared to 35 mg/g for BMSD. This suggests that the UMSD has a slightly higher affinity for lead ions than the base-treated seed, possibly due to differences in the surface chemistry and availability of active adsorption sites.

Fig. 11 illustrates the relationship between initial lead concentration and the adsorption capacity of two bioadsorbents: UMSD and BMSD. The data reveal a clear trend where the adsorption capacity of both bioadsorbents increases with rising initial lead concentrations.

Initially, both UMSD and BMSD exhibit similar adsorption capacities, indicating that at lower lead concentrations, the available adsorption sites on both adsorbents are sufficient to capture the majority of lead ions (Figs. 10 and 11). However, as the lead concentration increases, the competition for available sites intensifies, revealing the superior performance of UMSD. The enhanced adsorption capacity of UMSD at higher concentrations may be attributed to the retention of natural functional groups, such as hydroxyl (–OH) and carboxyl (–COOH) groups, on the surface of UMS, which are known to facilitate ion binding. In contrast, the chemical modification of BMS through NaOH treatment may have altered, masked, or reduced the accessibility of these functional groups, diminishing their adsorption efficiency.

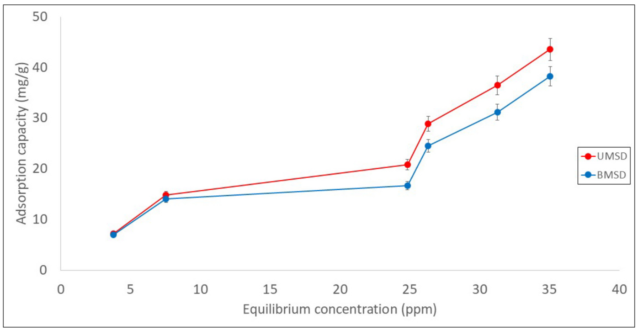

Fig. 10 Equilibrium concentration vs. adsorption capacity of UMSD and BMSD (the equilibrium conditions is 0.04 g bioadsorbent dosage, 400 rpm mixing rate, 120 min contact time, and pH range of 5–6.5)

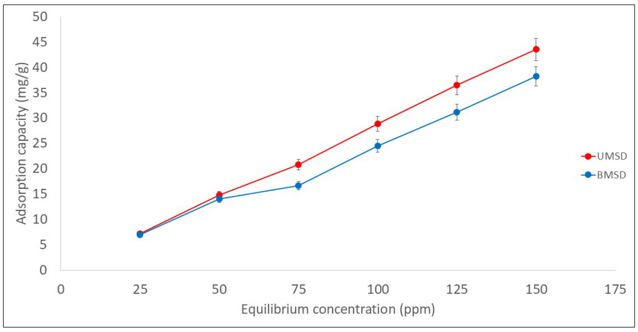

Fig. 11 Initial concentration vs. adsorption capacity of UMSD and BMSD (the equilibrium conditions is 0.04 g bioadsorbent dosage, 400 rpm mixing rate, 120 min contact time, and pH range of 5–6.5)

This finding is significant as it underscores the potential of UMSDs as an effective and low-cost bioadsorbent for lead removal from aqueous solutions. The superior performance of UMSD over BMSD at higher concentrations suggests that the base treatment process may alter the surface properties of the MSD in a way that reduces its adsorption efficiency. These results contribute to the broader understanding of how surface modifications can impact the effectiveness of bioadsorbents and highlight the importance of optimizing these treatments to maximize adsorption capacity.

3.6 Influence of varying contact times

As the adsorption time was systematically varied from 5 to 60 min, distinct trends in the adsorption capacity of both bioadsorbents were observed (Fig. 12). Initially, the adsorption capacity exhibited a noticeable increase for both the UMSD and the BMSD. Specifically, for UMSD, the adsorption capacity rose from 14 mg/g at the 5-min mark to 25 mg/g after just 15 min of contact time. This rapid increase in capacity suggests that the UMSD surface contains a significant number of active sites readily available for adsorption in the early stages of the process [23]. Similarly, BMSD demonstrated a comparable trend, with the adsorption

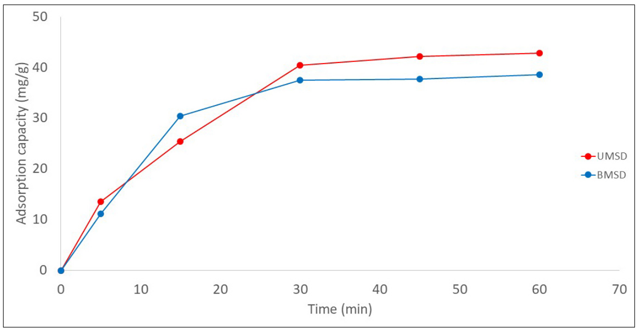

Fig. 12 Time vs. adsorption capacity of UMSD and BMSD (the equilibrium conditions is 100 ppm lead concentration, 0.04 g bioadsorbent dosage, 400 rpm mixing rate, 120 min contact time, and pH range of 5–6.5)

capacity increasing from 11 mg/g at 5 min to 30 mg/g at the 15-min interval. The more pronounced rise in capacity for BMSD compared to UMSD during the initial 15 min indicates that the base treatment may have enhanced certain surface characteristics, such as the density or exposure of active adsorption sites, potentially improving the initial interaction between the adsorbent and the lead ions.

As the adsorption time continued to increase, the capacity for both bioadsorbents continued to rise, albeit at a diminishing rate. For UMSD, the adsorption capacity reached approximately 40.5 mg/g at the 30-min mark, while BMSD showed a slightly lower capacity of 38 mg/g at the same time. This ongoing increase suggests that the adsorption process was still actively occurring, with additional adsorption sites being occupied as time progressed. However, beyond the 30-min point, the increase in adsorption capacity became minimal. This plateau in capacity indicates that the adsorption sites on the surfaces of both UMSD and BMSD were nearing saturation. The surface of the adsorbent likely reached a point where the number of available binding sites for the adsorbate was insufficient to facilitate significant additional adsorption. As a result, the adsorption capacity levels off, and further increases in time produce only minor changes.

3.7 Determination of isotherm model

The diminishing increase in adsorption capacity beyond 30 min aligns with typical adsorption kinetics [24], where the adsorption process slows as equilibrium approaches. The reduction in available binding sites and the accumulation of adsorbed ions on the surface may also create steric hindrance, further limiting the adsorption of additional ions. Thus, the plateau suggests that the bioadsorbents had reached their near-maximum adsorption capacity under the given experimental conditions.

Fig. 13 shows the adsorption data and their linear fit to the Langmuir and Freudlich models. The data reveals in Table 1 that both UMSD and BMSD exhibit a stronger alignment with the Langmuir equation, as indicated by their higher coefficients of determination (R^2) values of 0.97 and 0.93, respectively, compared to the Freundlich model, where the R^2 values are 0.95 and 0.87. This suggests that the adsorption process on these biosorbents is better characterized by the Langmuir isotherm, which assumes monolayer adsorption on a homogeneous surface [5, 25]. This indicates that the adsorption process on UMSD and BMSD follows a predictable saturation behavior, where all adsorption sites are equally accessible and occupied by a single layer of lead ions.

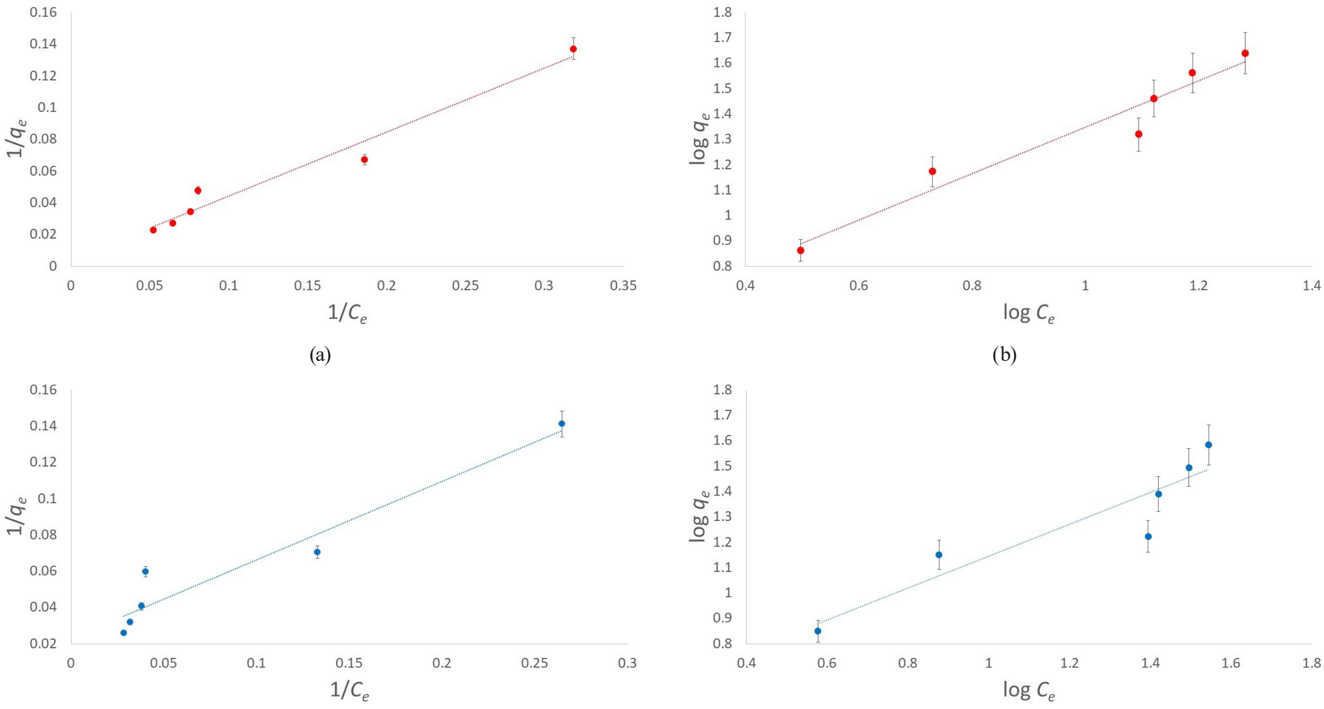

(a) (b)

(c) (d)

Fig. 13 Adsorption isotherms of UMSD and BMSD: (a) UMSD Langmuir; (b) UMSD Freundlich; (c) BMSD Langmuir; (d) BMSD

Table 1 Isotherm parameters for adsorption

UMSD				BMSD			
Langmuir		Freundlich		Langmuir		Freundlich	
K_L	0.0097	K_F	0.40	K_L	0.05	K_F	0.28
q_m	256.41 mg/g	$1/n$	0.92	q_m	43.54 mg/g	$1/n$	0.63
R^2	0.97	R^2	0.95	R^2	0.93	R^2	0.87

The Langmuir isotherm model's superior fit, particularly for the adsorption of Pb^{2+} ions, challenges the typical expectation that bioadsorbents, due to their heterogeneous nature, would more closely follow the Freundlich model, which accounts for multilayer adsorption on heterogeneous surfaces. It was reported that as the particle size of the biosorbent decreases the surface area increases which favors the Langmuir model [25]. As the surface area of UMSD and BMSD expands with smaller particle sizes, the distribution of active sites may become more homogeneous, favoring the formation of a monolayer of lead ions. This shift in adsorption behavior toward the Langmuir model implies that particle size and surface morphology are critical variables that can influence adsorption mechanisms.

These observations are consistent with prior studies, which also found the Langmuir isotherm to provide a better fit for adsorption processes involving heavy metals [26]. These studies support the conclusion that the Langmuir model is particularly suited to systems where the adsorbent surface behaves uniformly, allowing for the formation of a monolayer of adsorbate molecules.

The results from this study not only confirm the Langmuir model's relevance for Pb^{2+} adsorption on UMSD and BMSD but also highlight the importance of considering adsorbent surface characteristics, particle size, and morphology when selecting the appropriate isotherm model for adsorption studies.

3.8 Determination of kinetic model

To determine the appropriate kinetic model for the adsorption process, the analyzed data from experiments with varying contact times by employing two distinct approaches. First, plotted time against the natural logarithm of the difference between the equilibrium adsorption capacity and the adsorption capacity at each given time to assess the fit for pseudo-first-order kinetics (Fig. 14 (a)). This approach assesses the fit of the data to a model where the adsorption rate is proportional to the difference between the amount adsorbed at equilibrium and at any given time.

Second, plotted time versus the time divided by the adsorption capacity at each time point to evaluate pseudo-second-order kinetics (Fig. 14 (b)). These analyses enabled us to identify which kinetic model most accurately describes the adsorption behavior of the system.

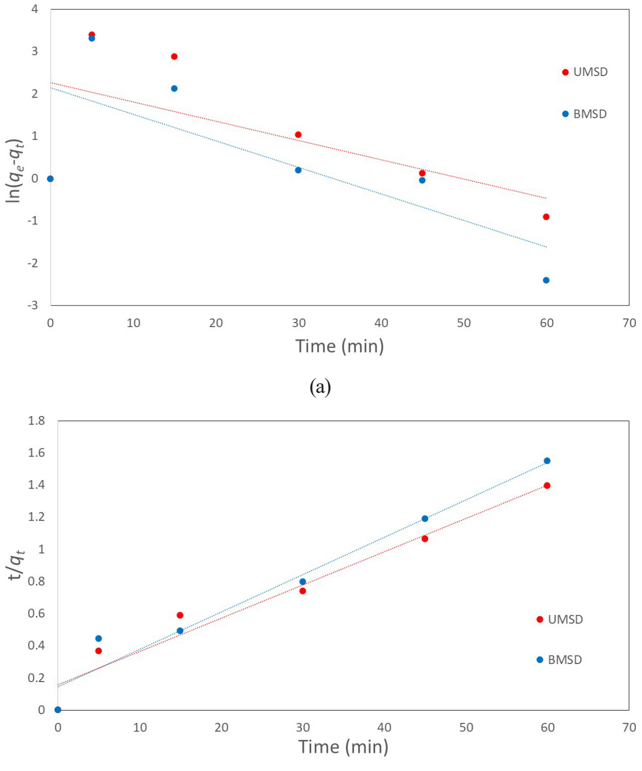

(a)

(b)

Fig. 14 Linearized kinetic models of UMSD and BMSD: (a) pseudo first-order; (b) pseudo second-order

Table 2 presents the kinetic parameters derived from experiments with contact times ranging from 5 to 60 min, with a 75-min duration used as the standard for determining equilibrium adsorption capacity. The experimental results reveal that both the UMSD and the BMSD conform to pseudo-second-order kinetics, which is a model often used to describe adsorption processes. This conclusion is substantiated by the high coefficients of determination (R^2) observed for each bioadsorbent. Specifically, the R^2 value for UMSD is 0.96, while for BMSD, it is 0.96. Pseudo-second-order kinetics is characterized by a rate law where the adsorption rate is dependent on the square of the amount of adsorbate adsorbed or, equivalently, on the

Table 2 Kinetic parameters for adsorption

Kinetic model	UMSD $q_{e(\mathrm{exp})}$ = 43.33 mg/g		BMSD $q_{e(\mathrm{exp})}$ = 38.76 mg/g	
Pseudo first-order	$q_{e(\mathrm{cal})}$	9.63 mg/g	$q_{e(\mathrm{cal})}$	8.63
	K_1	0.05	K_1	−0.0010
	R^2	0.39	R^2	0.56
Pseudo second-order	$q_{e(\mathrm{cal})}$	47.98 mg/g	$q_{e(\mathrm{cal})}$	42.92 mg/g
	K_2	0.0000	K_2	0.0037
	R^2	0.96	R^2	0.96

number of active sites available for binding This model assumes that the rate-determining step of the adsorption process involves the interaction between adsorbate molecules and the adsorption sites on the adsorbent surface [27]. The high R^2 values suggest that the adsorption processes for both UMSD and BMSD are well-described by this model, implying that the adsorption rate is primarily controlled by the chemical interactions between the adsorbate and the adsorbent.

From the previous research of absorption of Pb^{2+} ion from bio adsorbents seen in Table 3 [7, 28].

Compared from the past studies with the highest adsorption capacity of the MSD relatively low due to the composition and the structure of the seeds of mango than the other waste product. However, in the bright side this study proves that the UMSD may be modest to medium absorbent capabilities. Further studies on the optimization may be tested for higher absorbent capability.

Table 3 Bio adsorption of Pb^{2+} of different biomass

Material	Adsorption capacity (mg/g)	Reference
UMSD	42.10	This study
UMPL	37.36	This study
BMSD	38.38	This study
Merlot grape	40.1	[28]
Sauvignon Blanc grape marc	63.8	[28]
Raw apple waste	44.6	[7]
Extracted apple waste	48.6	[7]

4 Conclusion

In conclusion, this study demonstrates that mango waste-derived bioadsorbents, particularly UMSDs, offer an effective, low-cost, and sustainable solution for removing lead from wastewater. The UMSD exhibited superior adsorption performance, reaching capacities exceeding 42 mg/g, highlighting the efficiency of its natural functional groups in lead binding. Characterization *via* FTIR and SEM confirmed significant surface modifications and the presence of functional groups critical to adsorption. The adsorption followed the Langmuir isotherm model, indicating monolayer adsorption, with kinetics governed by a pseudo-second-order mechanism, emphasizing the role of chemical interactions. The findings underscore the potential of using UMSDs as a practical bioadsorbent for environmental remediation, providing a green alternative for managing lead contamination in water resources.

References

[1] Satyam, S., Patra, S. "Innovations and challenges in adsorption-based wastewater remediation: A comprehensive review", Heliyon, 10(9), e29573, 2024. https://doi.org/10.1016/j.heliyon.2024.e29573

[2] Moghimi Dehkordi, M., Pournuroz Nodeh, Z., Soleimani Dehkordi, K., Salmanvandi, H., Rasouli Khorjestan, R., Ghaffarzadeh, M. "Soil, air, and water pollution from mining and industrial activities: Sources of pollution, environmental impacts, and prevention and control methods", Results in Engineering, 23, 102729, 2024. https://doi.org/10.1016/j.rineng.2024.102729

[3] Latiza, R. J. P., Mustafa, A., Delos Reyes, K., Nebres, K. L., Rubi, R. V. C. "Adsorbents Derived from Plant Sources for Caffeine Removal: Current Research and Future Outlook", Engineering Proceedings, 67(1), 15, 2024. https://doi.org/10.3390/engproc2024067015

[4] Sud, D., Mahajan, G., Kaur, M. P. "Agricultural waste material as potential adsorbent for sequestering heavy metal ions from aqueous solutions – A review", 99(14), pp. 6017–6027, 2008. https://doi.org/10.1016/j.biortech.2007.11.064

[5] Kanjilal, T., Babu, S., Biswas, K., Bhattacharjee, C., Datta, S. "Application of mango seed integuments as bio-adsorbent in lead removal from industrial effluent", Desalination and Water Treatment, 56(4), pp. 984–996, 2015. https://doi.org/10.1080/19443994.2014.950999

[6] Abdelaziz, S. A. "Physico chemical characteristics of mango kernel oil and meal", Middle East Journal of Applied Sciences, 8(1), pp. 1–6, 2018.

[7] Ungureanu, G., Enache, I.-M., Cara, I. G., Motrescu, I., Patras, A. "Insights into the environmental benefits of using apple pomace for biosorption of lead from contaminated water", Heliyon, 10(17), e36811, 2024. https://doi.org/10.1016/j.heliyon.2024.e36811

[8] Saravanan, A., Karishma, S., Kumar, P. S., Thamarai, P., Yaashikaa, P. R. "Recent insights into mechanism of modified bio-adsorbents for the remediation of environmental pollutants", Environmental Pollution, 339, 122720, 2023. https://doi.org/10.1016/j.envpol.2023.122720

[9] Tsaniatri, D. A., Hargono, H. "Adsorption of Pb(II) from aqueous solution by acid-modified water hyacinth cellulose", IOP Conference Series: Materials Science and Engineering, 1053(1), 012010, 2021. https://doi.org/10.1088/1757-899x/1053/1/012010

[10] Iqbal, M., Saeed, A., Kalim, I. "Characterization of Adsorptive Capacity and Investigation of Mechanism of Cu^{2+}, Ni^{2+} and Zn^{2+} Adsorption on Mango Peel Waste from Constituted Metal Solution and Genuine Electroplating Effluent", Separation Science and Technology, 44(15), pp. 3770–3791, 2009. https://doi.org/10.1080/01496390903182305

[11] Department of Environment and Natural Resources (DENR) "DENR Administrative Order No. 2021-19 Updated Water Quality Guidelines (WQG) and General Effluent Standards (GES) for Selected Parameters", [pdf] Department of Environment and Natural Resources, Quezon City, Republic of Philippines, 2021. Available at: https://faolex.fao.org/docs/pdf/phi214300.pdf [Accessed: 27 March 2025]

[12] Department of Environment and Natural Resources (DENR) "General Effluent Standards (GES)", [pdf] Department of Environment and Natural Resources, Quezon City, Republic of Philippines, 2016. Available at: https://www.denr.gov.ph [Accessed: 24 October 2024]

[13] Eguico, C. S., Abanto, M. M., Cendaña, H. T., Perez Famero, D. A., Pediongco, K. B., Cruz Evangelista, A. D., Del Castillo Rubi, R. V. "Sonophotopythochemical Functionalization of Graphene Oxide - Al - Zn Bimetal Nanocomposite for Corrosion Inhibition", Applied Science and Engineering Progress, 18(2), 7613, 2025. https://doi.org/10.14416/j.asep.2024.10.004

[14] Ul Haq, H., Elik, A., Isci, G., Ekici, M., Gürsoy, N., Boczkaj, G., Altunay, N. "Development of a vortex-assisted switchable-hydrophilicity solvent-based liquid phase microextraction for fast and reliable extraction of Zn (II), Fe (II), Pb (II), and Cd (II) from various baby food products", Food Chemistry, 447, 139024, 2024. https://doi.org/10.1016/j.foodchem.2024.139024

[15] Cruz-Lopes, L. P., Macena, M., Esteves, B., Guiné, R. P. F. "Ideal pH for the adsorption of metal ions Cr^{6+}, Ni^{2+}, Pb^{2+} in aqueous solution with different adsorbent materials", Open Agriculture, 6(1), pp. 115–123, 2021. https://doi.org/10.1515/opag-2021-0225

[16] Dehghani, M. H., Afsari Sardari, S., Afsharnia, M., Qasemi, M., Shams, M. "Removal of toxic lead from aqueous solution using a low-cost adsorbent", Scientific Reports, 13(1), 3278, 2023. https://doi.org/10.1038/s41598-023-29674-x

[17] Zakaria, A., Aynuddin, A., Djasmasari, W. "Exploring The Potential of Mango Seed as A Bioadsorbent for Pb(II) Removal in Aqueous Solution", Jurnal Kimia Valensi, 9(1), pp. 155–162, 2023. https://doi.org/10.15408/jkv.v9i1.31733

[18] Huang, W., Yang, Z., Hu, J., Chen, X., Li, W., Wang, Z., Zhang, C., Wang, Q., Xiao, X., Yu, P. "Mechanisms and valorization of selective adsorption of Sb(III) by amino-functionalized lignin-based porous biochar", Chemical Engineering Journal, 499, 156262, 2024. https://doi.org/10.1016/j.cej.2024.156262

[19] Gieroba, B., Kalisz, G., Krysa, M., Khalavka, M., Przekora, A. "Application of Vibrational Spectroscopic Techniques in the Study of the Natural Polysaccharides and Their Cross-Linking Process", International Journal of Molecular Sciences, 24(3), 2630, 2630. https://doi.org/10.3390/ijms24032630

[20] Somyanonthanakun, W., Ahmed, R., Krongtong, V., Thongmee, S. "Studies on the adsorption of Pb(II) from aqueous solutions using sugarcane bagasse-based modified activated carbon with nitric acid: Kinetic, isotherm and desorption", Chemical Physics Impact, 6, 100181, 2023. https://doi.org/10.1016/j.chphi.2023.100181

[21] Kučuk, N., Primožič, M., Kotnik, P., Knez, Ž., Leitgeb, M. "Mango Peels as an Industrial By-Product: A Sustainable Source of Compounds with Antioxidant, Enzymatic, and Antimicrobial Activity", Foods, 13(4), 553, 2024. https://doi.org/10.3390/foods13040553

[22] Tetteh, I. K., Issahaku, I., Tetteh, A. Y. "Recent advances in synthesis, characterization, and environmental applications of activated carbons and other carbon derivatives", Carbon Trends, 14, 100328, 2024. https://doi.org/10.1016/j.cartre.2024.100328

[23] Zaimee, M. Z. A., Sarjadi, M. S., Rahman, M. L. "Heavy Metals Removal from Water by Efficient Adsorbents", Water, 13(19), 2659, 2021. https://doi.org/10.3390/w13192659

[24] Benjelloun, M., Miyah, Y., Akdemir Evrendilek, G., Zerrouq, F., Lairini, S. "Recent Advances in Adsorption Kinetic Models: Their Application to Dye Types", Arabian Journal of Chemistry, 14(4), 103031, 2021. https://doi.org/10.1016/j.arabjc.2021.103031

[25] Murphy, O. P., Vashishtha, M., Palanisamy, P., Kumar, K. V. "A Review on the Adsorption Isotherms and Design Calculations for the Optimization of Adsorbent Mass and Contact Time", ACS Omega, 8(20), pp. 17407–17430, 2023. https://doi.org/10.1021/acsomega.2c08155

[26] Chen, X., Hossain, M. F., Duan, C., Lu, J., Tsang, Y. F., Islam, M. S., Zhou, Y. "Isotherm models for adsorption of heavy metals from water - A review", Chemosphere, 307, 135545, 2022. https://doi.org/10.1016/j.chemosphere.2022.135545

[27] Ahmed Alsharif, M. "Understanding Adsorption: Theories, Techniques, and Applications", In: Shabatina, T. (ed.) Adsorption - Fundamental Mechanisms and Applications, IntechOpen, 2025, pp. 3–10. ISBN 978-1-83634-490-2 https://doi.org/10.5772/intechopen.1008865

[28] Ungureanu, G., Patras, A., Cara, I. G., Sturza, R., Ghendov-Mosanu, A. "Innovative Recovery of Winemaking Waste for Effective Lead Removal from Wastewater", Agronomy, 12(3), 604, 2022. https://doi.org/10.3390/agronomy12030604